Driving force induced transition in thermal behavior of grain boundary migration in Ni

Xinyuan Song and Chuang Deng [*]

Department of Mechanical Engineering, University of Manitoba, Winnipeg, Manitoba, Canada R3T 2N2

Grain boundary (GB) migration exhibits intriguing antithermal behavior (or non-Arrhenius behavior), with the temperature and driving force playing crucial roles. Through atomistic simulations on nickel bicrystals, we investigate the change in GB mobility with variations in both temperature and driving force. Our results reveal that the GB mobility initially increases with temperature and subsequently decreases after reaching the transition temperature (T_{trans}), and, notably, T_{trans} exhibits a linear relationship with the activation energy (Q) associated with GB migration. By modulating the driving force, we found that the driving force could effectively lower Q, resulting in the shift of T_{trans} towards lower temperatures. Additionally, higher driving forces were found to activate more migration modes at lower temperatures, potentially leading to a transition in the thermal behavior of GB migration. Our work supports the existing theoretical models for GB migration based on both classical thermal activation and disconnection nucleation. Furthermore, we refined the existing model by incorporating the influence of the driving force. The modified model can not only describe the effect of driving force on the thermal behavior of GB migration but also accounts for the observed "antidriving force" phenomenon in GB migration. Our research has the potential to offer valuable insights for investigating realistic GB migration under more intricate constraints and environments.

I. INTRODUCTION

Grain boundary (GB) mobility is a fundamental dynamic property that characterizes the rate at which a GB moves in response to an external driving force, which is an important parameter that influences the microstructural evolution of polycrystalline materials. Despite the apparent physical meaning of GB mobility and extensive investigations conducted through experiments [1–4] and atomistic simulations [5–14], accurately predicting GB migration behavior remains challenging due to the complexity arising from the five-parameter space associated with GBs. While numerous theoretical models, such as those based on the conventional concepts of the structural unit [15,16] and the more recent ones based on machine learning and the various types of local atomic descriptors [17,18], have been developed to successfully predict other fundamental properties of GBs, such as GB energy [18] and the energy spectrum for solute segregation [17], no such model can accurately forecast the migration behavior of GBs, even for GB structures of high symmetry. Therefore, a profound understanding of GB migration behavior and the corresponding predictive theory are highly desired in the community and hold significant importance for modern manufacturing industries [19].

The migration of GBs has traditionally been considered thermally activated, following the empirical Arrhenius relation [4,20]: $M = M_0 \exp(-Q/k_B T)$, where M_0 is a constant prefactor, Q is the activation energy, k_B is the Boltzmann constant, and T is the temperature. However, in recent years, the phenomenon of antithermal behavior (or non-Arrhenius behavior) in GBs has been widely reported, which refers to the decrease in GB mobility with increasing temperature. For instance, atomistic studies [10–12] have indicated the prevalence of antithermal behavior in specific GBs, such as $\Sigma 3$, $\Sigma 7$, and $\Sigma 9$ GBs in Ni. Experimental observations, as discussed in [4], have also reported faster GB migration at cryogenic temperatures [21] and slower GB migration at higher temperatures [22,23].

The mechanism underlying the antithermal behavior of GB migration remains a subject of ongoing debate. One hypothesis, put forth by Priedeman *et al.* [10], suggests that the slowdown in GB migration can be attributed to phonon drag, which is the mechanism that hinders the motion of dislocation. However, a recent study conducted by Homer *et al.* [24] presents a different perspective on the antithermal behavior of GB migration. They reintroduce the classical thermal-activation model originally proposed by Gottstein and Shvindlerman [25] and argue that the observed deceleration of GB migration at lower temperatures is a thermal activation phenomenon rather than an external influence. Additionally, Chen *et al.* [7] propose a theoretical model based on disconnection theory, providing further support for the notion that the antithermal behavior is an inherent characteristic of GBs. Several other hypotheses have also been put forward, such as structural phase transitions [26,27], roughening transitions [8,28], and topological phase transitions [29]. However, further investigations are needed to substantiate these hypotheses.

The classical kinetic equation for GB migration is given by

$$v = MP|_{P \to 0} \tag{1}$$

[*]Chuang.Deng@umanitoba.ca

where v is the velocity of the GB motion and P is the driving force, and M is the GB mobility. According to this equation, the GB mobility should be independent of the driving force when the driving force approaches zero [30]. However, in previous studies using molecular dynamics (MD) simulations, relatively large driving forces were applied to observe GB migration within the nanosecond time scale. This approach has a great effect on the measured mobility [11,12] and thermal behavior of GBs [11]. For instance, as reported in [11], when the applied driving force for the Ni $\Sigma 7$ (5 4 1)/(5 4 $\bar{1}$) GB (P26 in the Olmsted database [31]) changes from 74 to 372 MPa, the GB migration behavior transitions from thermally activated to antithermal. With the same change in driving force, the $\Sigma 7$ (8 5 1)/(7 5 4) GB (P207 in the Olmsted database [31]) exhibits a transition from antithermal to thermally activated migration behavior. This dependency of thermal behavior on the driving force complicates the study of thermal behavior of GB and direct comparisons between experimental observations (typically performed with driving forces in the range 10^2–10^6 Pa [32]) and atomistic simulations (with driving forces typically larger than 10^7 Pa [11]). To date, no systematic research has been conducted to investigate the effect of the driving force on the thermal behavior of GB migration, further emphasizing the need for comprehensive studies in this area.

Trautt *et al.* [9] have proposed a method to extract GB mobility at the zero-driving force limit from the random walk of the GB. Deng and Schuh [33] further enhanced the accuracy of this method, enabling it to capture the subtle movements of GBs more effectively. According to this approach, the mobility of a flat and fully periodic GB can be computed using the Einstein relation [9],

$$D = 2Mk_BT/A, \qquad (2)$$

where A represents the GB area and D is the GB diffusion coefficient. It is important to note that D, in this context, is based on the mean square displacement (MSD) of the average normal migration of the entire GB plane. This is distinct from the conventional GB diffusivity, which tracks the MSD of individual GB atoms, although these two properties may be fundamentally correlated. At low temperatures, GBs are expected to exhibit neglectable movement due to the limited thermal fluctuations. As a result, the random walk method has primarily been utilized to compute GB mobility in the high-temperature regime (typically above 500 K) in previous studies [9,34]. However, in a recent study by Homer *et al.* [24], it was demonstrated that the antithermal behavior of GB migration is likely associated with small activation energies for GB migration, which implies that the random walk of these GBs can be obvious at low temperatures.

In this paper, we aim to investigate the thermal behaviors of GBs with different activation energies using the interface random walk method. This approach will help determine whether the antithermal GB migration is an intrinsic property of GBs or a thermal phenomenon induced by external driving forces. Furthermore, by using the mobility and thermal behavior of GBs obtained through the random walk method as a reference, the study systematically explores the influence of external driving forces on the activation barriers for GB migration and the thermal behavior of GBs. The findings of this investigation are subsequently compared with existing theoretical models,
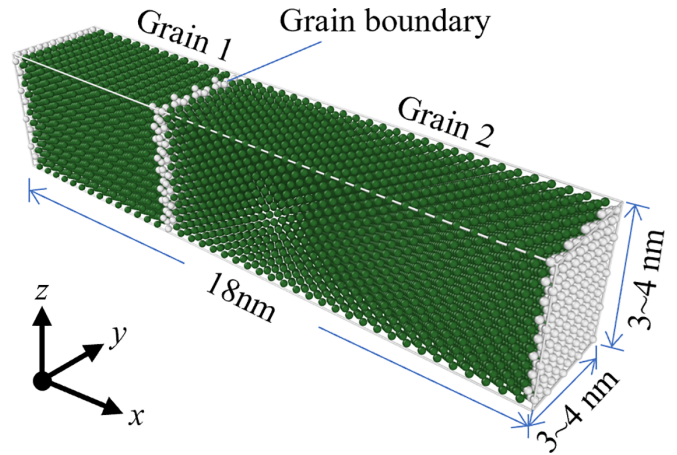

FIG. 1. A representative atomistic model of the simulated Ni GBs. Atoms located at perfect FCC sites and non-FCC sites are color-coded in green and white, respectively.

and the effects of driving forces are discussed. The aim of this study is to shed light on the physical mechanisms underlying the thermal behavior of GB migration and to illustrate how external driving forces can play a role.

II. METHOD

A. GB data set

In order to investigate the relationship between activation energy and the thermal behavior of GB migration, we have selected nine coincidence site lattice (CSL) Ni GB models from the Olmsted database [31]. These GB models are known to potentially exhibit small activation energies for migration based on previous studies [11,35]. Two methods are employed to compute the activation energy of the GBs: The first method involvs fitting the $\ln M$-$1/k_B T$ line to calculate the apparent activation energy, denoted as Q. This method will be discussed in detail in Sec. IV B. The second method uses nudged elastic band (NEB) methods [36–38] to compute the energy barrier during GB migration, denoted as E. See the Supplemental Material [39] for the detailed procedure for computing the energy barriers [36–38,40–42]. This method has been widely used in previous research on GB migration [7,43,44]. Figure 1 illustrates a typical GB model, and Table I provides detailed information about each GB. To study the "intrinsic" thermal behavior of GB migration and the influence of the driving force, the boundary condition in the x direction is set as shrink-wrapped (free surfaces) to eliminate constraints and other factors that could affect GB migration, except for temperature and driving force. The boundary conditions in the y and z directions (GB plane directions) are set as periodic. All simulations are performed using the Large-scale Atomic/Molecular Massively Parallel Simulator (LAMMPS) package [45] with an embedded atom method (EAM) potential [46]. The simulations are conducted within the temperature range 10–800 K and, in some cases, up to 1000 K.

TABLE I. The detailed information on the GBs investigated in this study, specifically their energy barriers for GB migration E and apparent activation energy Q. The E are presented in ascending order from low to high values. Some GBs show two energy barriers during the migration (E) as discussed in Sec. IV B.

ID in the Olmsted database [31]	Sigma	GB plane	Energy barrier for GB migration E (eV/nm$^2 \times 10^{-3}$)	Apparent activation energy Q (eV)
207	7	(8 5 1)/(7 5 4)	0.61	0.0024
256	87	(11 7 2)/(11 7 2)	2.36	0.0054
87	9	(7 5 4)/(7 5 $\bar{4}$)	2.84	0.0076
57	35	(4 2 0)/(4 2 0)	3.37	0.0078
167	35	(10 6 2)/(10 6 2)	4.73	0.027
257	29	(11 7 2)/(11 7 $\bar{2}$)	5.42	0.046
25	21	(5 4 1)/(5 4 1)	7.97	0.072
30	3	(3 2 1)/(3 2 $\bar{1}$)	0.29/5.08	Almost 0
14	15	(2 1 1)/(2 1 1)	1.89/6.67	0.018

B. Random walk simulation

Before tracking the GB migration, the models were expanded at different temperatures based on the corresponding thermal expansion coefficient. Subsequently, equilibration was performed under the isothermal-isobaric ensemble (*NPT*) for 10 ps, followed by a short annealing period of 5 ps under the microcanonical ensemble (*NVE*) using the Berendsen thermostat. The Berendsen thermostat was then removed, and the GBs were left to fluctuate randomly for 5 ns solely under the thermal effects in the *NVE* ensemble. The variation in the order parameter, as described in Ref. [47], was employed to track the mean position across the GB plane within the system. Additionally, to determine the shear coupling factor during the thermal fluctuations of each GB, the relative shear displacement in each model was recorded, by tracking the center of mass of a thin slab, approximately 1 nm thick, at both ends along the x direction. To ensure the reliability of the results, each simulation was repeated 20 times with different random seeds for the initial velocity distribution. The duration of each simulation was 5 ns, and the resulting data sets were split into ten groups of 500 ps, resulting in a total of 200 sets of independent simulation results for each condition. Figure 2
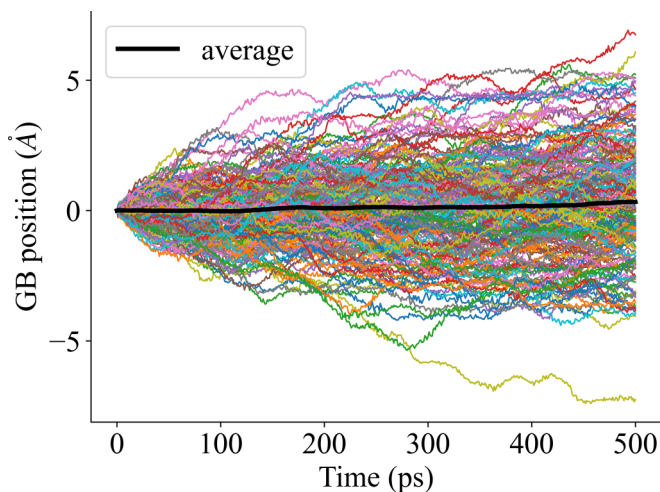
illustrates an example of GB migration across 200 simulations. The initial GB position was defined as 0 for all simulations. It was observed that even at a low temperature of 200 K, the GB with a $\Sigma 15$ (2 1 1) structure exhibited detectable migration solely due to thermal effects. The GB migration was found to be entirely random, with the average position (indicated by the thick black line) remaining in the middle.

For each simulation, the cumulative distribution function $f(x)$ [33] at a given time t can be described by the following equation:

$$f(x) = \frac{1}{2}\left[1 + \text{erf}\left(\frac{x - \mu}{\sigma\sqrt{2}}\right)\right], \tag{3}$$

where $f(x)$ is the probability that the displacement of the mean position across the GB plane, denoted as $d(t)$, falls within the range $(\infty, x]$, and erf is the error function. The fitted parameters μ corresponds to the average displacement $\langle \bar{d}(t) \rangle$, and σ^2 corresponds to the mean square displacement $\langle \bar{d}^2(t) \rangle = Dt$. Therefore, D can be calculated by $d\sigma^2/dt$, and the GB mobility M can be determined using Eq. (2).

C. External driving force driven GB migration

The effect of the driving force on GB migration was investigated using the energy-conserving orientational (ECO) synthetic driving force [47,48]. As a point of comparison, the influence of shear stress was also examined by applying opposing shear forces on the two thin slabs at both ends along the x direction. Each GB was subjected to this driving force until it reached one end of the model, with a maximum simulation time of 5 ns. To ensure statistical significance, each simulation was repeated 20 times with different random seeds for initial velocity distribution.

The velocity of the GB in each simulation was determined by linearly fitting the displacement vs time curve through the least square error method [49] and calculating the slope of the fitted line. The final GB velocity was obtained by averaging the velocities from the 20 simulations. Based on the calculated velocity, the GB mobility was then determined using Eq. (1).
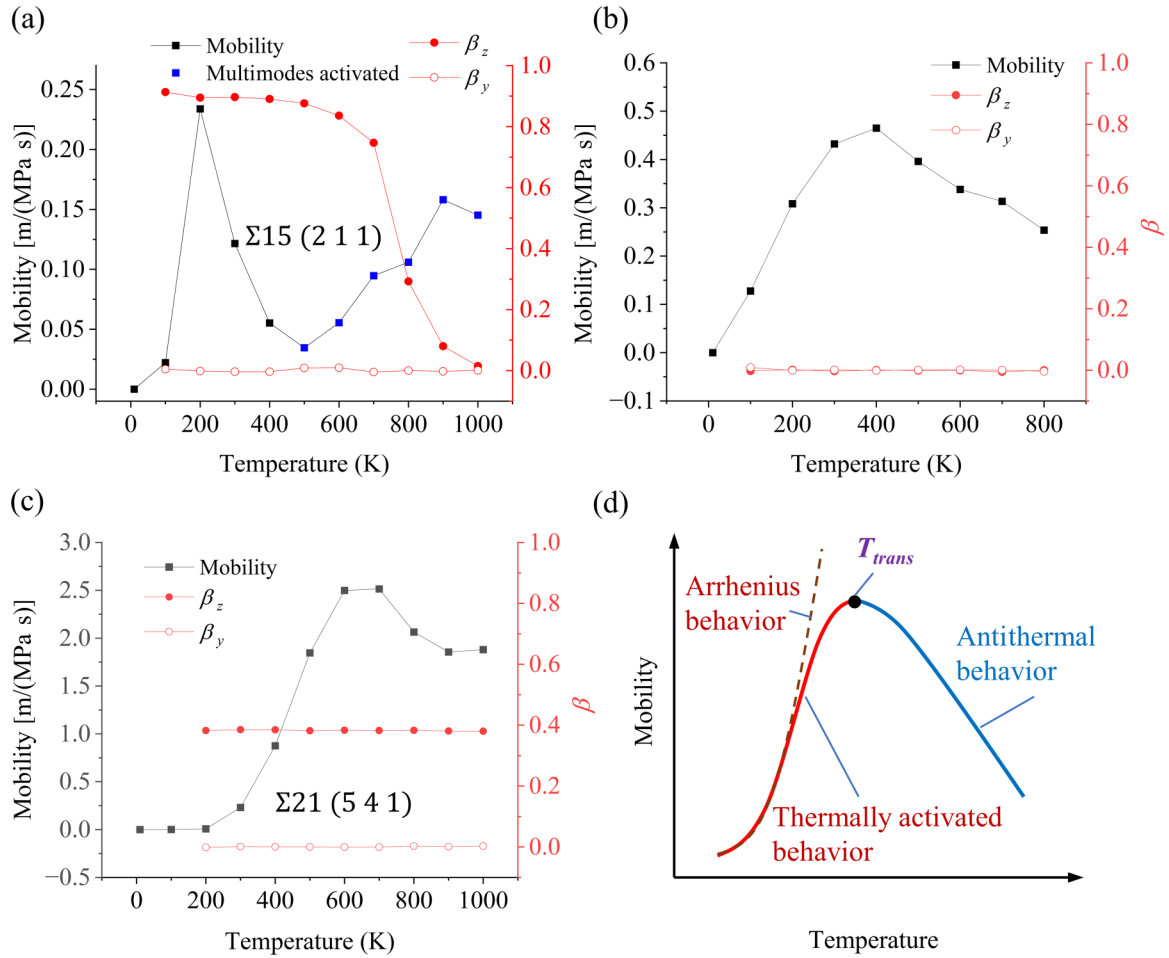

FIG. 2. The migration of $\Sigma 15$ (2 1 1) GB under the effect of thermal fluctuation at 200K.

FIG. 3. The plots of GB mobility and shear coupling factor vs. temperature determined from random walk simulation for (a) $\Sigma15$ (2 1 1) (the blue dots indicate a change in disconnection modes at specific temperatures), (b) $\Sigma9$ (7 5 4)/(7 5 $\bar{4}$) and (c) $\Sigma21$ (5 4 1) GBs. (d) Illustration of the thermally activated behavior (i.e., mobility increases with temperature), the anti-thermal behavior (i.e., mobility decreases with temperature), and the transition temperature T_{trans}.

III. RESULTS

A. Temperature-dependent GB mobility: Random walk simulations

In the random walk simulations, all nine GBs listed in Table I exhibited antithermal behavior in terms of GB mobility. The paper specifically focuses on three representative GBs, namely $\Sigma15$ (2 1 1), $\Sigma9$ (7 5 4)/(7 5 $\bar{4}$), and $\Sigma21$ (5 4 1) GBs, and their respective M vs T curves are shown in Figs. 3(a)–3(c) (see the Supplemental Material [39] for the M vs T curves of the remaining GBs). The results indicate that at low temperatures, the GB mobility displayed a thermally activated behavior, where higher temperatures led to increased mobility. However, as the temperature further increased, a transition occurred, and then the GB mobility exhibited antithermal behavior, as shown in Fig. 3(d). This transition point, represented as T_{trans}, marks the temperature at which the thermal behavior of GB migration undergoes a transition.

According to the unified GB kinetics model proposed by Han *et al.* [30], GBs can migrate through different modes, each characterized by a specific shear coupling factor β. The

dichromatic pattern analysis, presented in the Supplemental Material [39], reveals that the migration modes of $\Sigma15$ (2 1 1) and $\Sigma21$ (5 4 1) GBs exhibit different β. Consequently, monitoring the changes in β allows us to track the activation status of migration modes for $\Sigma15$ (2 1 1) and $\Sigma21$ (5 4 1) GBs during the migration process, as demonstrated in Figs. 3(a) and 3(c). On the other hand, for $\Sigma9$ (7 5 4)/(7 5 $\bar{4}$) GB, its migration modes either do not possess a shear coupling effect or consist of two similar modes with opposite β, indicating a final β of 0, which is consistent with the observation shown in Fig. 3(b).

For both $\Sigma15$ (2 1 1) and $\Sigma21$ (5 4 1) GBs, it was observed that only a single mode (indicated by the constant β) was detected around the T_{trans}. This indicates that the transition in thermal behavior is not caused by a change in the migration mode. Specifically, for the $\Sigma15$ (2 1 1) GB, the shear coupling factor begins to decrease at 500 K, suggesting the activation of multimodes at this temperature. This may be the underlying mechanism that leads to an increase in GB mobility after 500 K [as indicated by the blue data points in Fig. 3(a)] and another transition in thermal behavior, specifically from antithermal to thermally activated behavior.
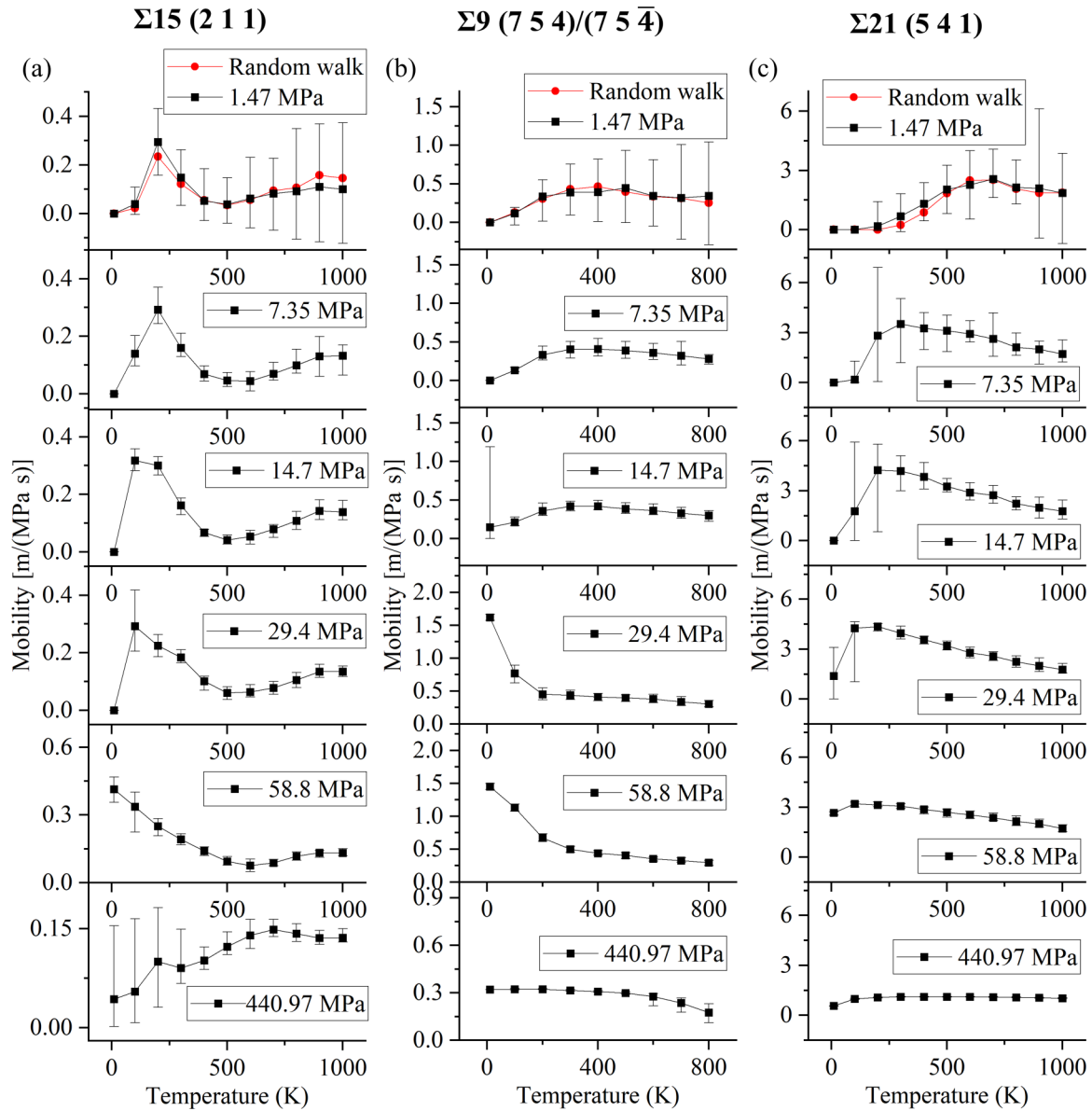
FIG. 4. The effect of synthetic driving force on GB mobility for (a) $\Sigma15$ (2 1 1), (b) $\Sigma9$ (7 5 4)/(7 5 $\bar{4}$), and (c) $\Sigma21$ (5 4 1) GBs in Ni.

B. Effect of driving force

The effect of the synthetic driving force on GB mobility is illustrated in Fig. 4. The large error bars observed at small driving forces indicate the stochastic nature of GB migration caused by random thermal fluctuations, as shown in Fig. 2. At low driving forces, such as 1.47 MPa, the GB mobility calculated using Eq. (1) closely matches that determined by the random walk method, consistent with previous findings [34]. As the driving force increases, the transition temperature T_{trans} for the thermal behavior of GB mobility shifts towards lower values. Notably, for $\Sigma15$ (2 1 1) and $\Sigma9$ (7 5 4)/(7 5 $\bar{4}$) GBs, the first peak in mobility completely disappears at driving forces of 58.8 and 29.4 MPa, respectively. Particularly for the $\Sigma9$ (7 5 4)/(7 5 $\bar{4}$) GB, a monotonic antithermal trend is observed when it is driven by this force up to 800 K. When the driving force reaches an extremely large value of 440.97 MPa, the mobility of $\Sigma9$ (7 5 4)/(7 5 $\bar{4}$) and $\Sigma21$ (5 4 1) GBs becomes essentially independent of temperature,

in agreement with the ballistic transition proposed by Deng and Schuh [32]. However, for $\Sigma15$ (2 1 1) GB, the mobility reverts back to a thermally activated behavior. This behavior requires further investigation and will be discussed in more detail below. Supplemental Material Fig. S4 [39] provides the M vs T curves for driving forces ranging 58.8–440.97 MPa, as well as the M vs P curves at different temperatures.

To investigate the underlying mechanisms behind the transition in thermal behavior of GB migration, the β for the $\Sigma15$ (2 1 1) GB under different driving forces and temperatures was analyzed and presented in Fig. 5. The heat map reveals that both a larger driving force and higher temperature can activate more migration modes during GB migration. Interestingly, when the synthetic driving force reaches 440.97 MPa, multiple modes can be activated even at very low temperatures, as low as 10 K. This observation may explain why the GB mobility of $\Sigma15$ (2 1 1) changes back to a thermally
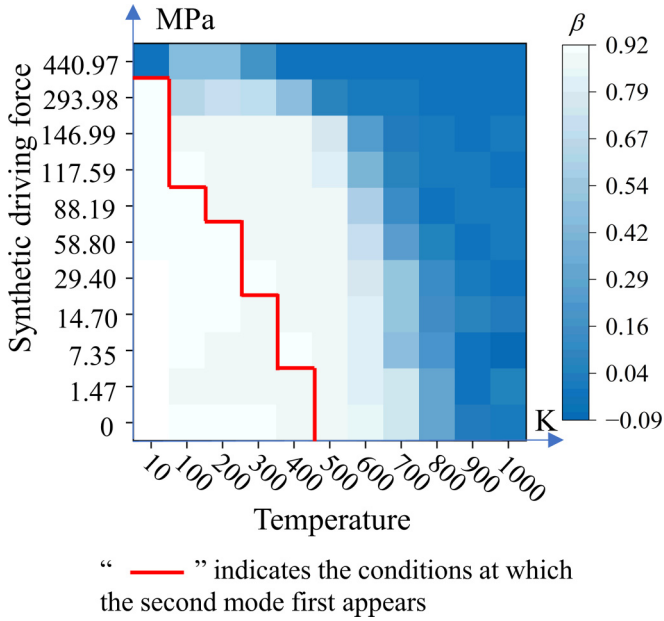
" —— " indicates the conditions at which
the second mode first appears

FIG. 5. Heatmap of the shear coupling factor in the $\Sigma 15$ (2 1 1) Ni GB under varying driving forces and temperatures.

FIG. 6. Mobility vs. driving force curves at 100 K and 800 K for $\Sigma 15$ (2 1 1) GB.

activated behavior [Fig. 4(a)] under the influence of a driving force of 440.97 MPa.

It is important to note that the T_{trans} in thermal behavior [Fig. 4(a)], occurring around 200 K and below for the cases when driving force $\leqslant 58.8$ MPa, do not correspond to the transition in migration modes shown in Fig. 5 (indicated by a red line). A similar phenomenon was also observed for the $\Sigma 21$ (5 4 1) GB [Fig. 3(c)], in which there is no change in β across all temperatures (10–1000 K), yet a peak in the GB mobility emerges around 700 K. Therefore, the transition from thermally activated to antithermal behavior in GB migration, as well as its dependence on driving force, cannot be solely attributed to the change in migration modes that are activated during the migration process.

In addition, another interesting observation is the presence of an "antithermal" trend in GB migration, or more accurately, an "antidriving force" trend, with increasing external driving forces. Figure 6 illustrates this behavior, where at a low temperature of 100 K, the mobility M of $\Sigma 15$ (2 1 1) GB initially increases and then decreases as the driving force increases. This trend is reminiscent of the antithermal phenomenon observed in GB mobility when the temperature changes under low driving force conditions (Fig. 4). In contrast, at a high temperature of 800 K, the GB mobilities remain nearly constant and do not exhibit a significant dependence on the driving force. A similar driving force-dependent "antithermal" trend in GB mobility has been reported in previous studies, such as those by Deng and Schuh [32] and Race *et al.* [50]. This intriguing phenomenon will be further discussed in the subsequent sections.

IV. DISCUSSION

A. Theoretical models for antithermal GB migration

The classical thermal-activation model, originally proposed by Gottstein and Shvindlerman [25] and recently
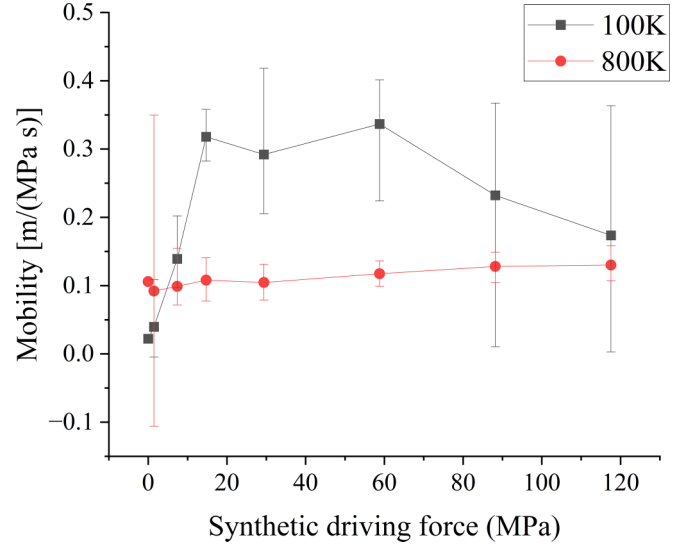
reintroduced by Homer *et al.* [24], offers an explanation for the antithermal behavior observed in GB migration. In this model, atoms randomly jump forth and back across the GB based on transition state theory, and a collective atom jump leads to GB migration. Figure 7(a) illustrates the model, where Q represents the activation energy for the atomic configuration transformation from S_1 to S_2, and Ψ represents the energy introduced by the external driving force. The velocity of the GB can be calculated using the equation

$$v = Nb \left[\omega^+ \exp \left(-\frac{Q}{k_B T} \right) - \omega^- \exp \left(-\frac{Q + \Psi}{k_B T} \right) \right]$$
$$= Nb\omega \exp \left(-\frac{Q}{k_B T} \right) \left[1 - \exp \left(-\frac{\Psi}{k_B T} \right) \right] \quad (4)$$

where N is the number of atoms, b is the distance of the atom jump, ω is the attempt frequency, $+$ and $-$ denote the forth and back directions of the GB migration. As the external driving force approaches 0, the terms in the square bracket in Eq. (4), i.e., $1 - \exp(-\Psi/k_B T)$ can be approximated as $\Psi/k_B T$. Since Ψ is the energy drop introduced by the external driving force and is proportional to the driving force P ($\Psi = CP$, where C is a constant), the GB mobility in the zero-driving force limit
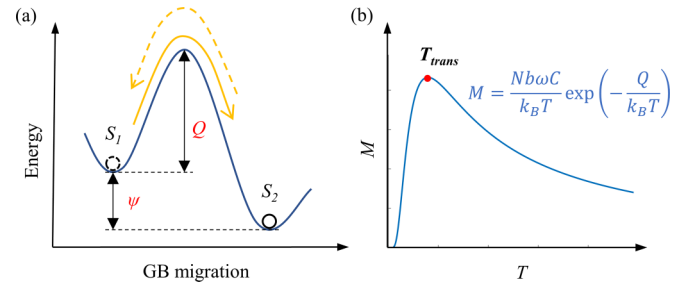

FIG. 7. (a) Illustration of the classical thermal-activation model [24] and (b) Plot of the mobility vs. temperature curve based on Eq. (5).

can be derived from Eq. (4) as

$$M = \frac{v}{P} = \frac{Nb\omega C}{k_B T} \exp\left(-\frac{Q}{k_B T}\right). \quad (5)$$

As shown in Fig. 7(b), Eq. (5) provides a good description of the antithermal behavior of GB migration. The GB mobility M initially increases with temperature T and after reaching its maximum value at T_{trans}, M starts to decrease as T further increases. This trend is consistent with the observations depicted in Figs. 3 and 4.

Chen *et al.* [7] also proposed an equation to describe the antithermal GB migration based on the disconnection theory, taking into account the activation and migration of disconnections. The equation is given as

$$M = \frac{2\omega\delta w}{k_B T} \sum_m \frac{h_m^2 \exp\left(-\frac{E_m^* + E_m^c}{k_B T/w}\right)}{1 + \frac{2}{e}\exp\left(\frac{E_m^e - 2E_m^c}{k_B T/w}\right)} \quad (6)$$

where w is the thickness of a bicrystal, δ is the size of a CSL cell, $e = \exp(1)$ is Euler's number, subscript m represents different disconnection modes, h is the height of the disconnection, E^C is the formation energy for a pair of disconnection, E^* is the energy barrier for disconnection migration along the GB, and E^e attributes to the long-range elastic interactions between disconnections. Due to the small magnitude of E^e compared to E^C, the denominator of the second fraction in Eq. (6), i.e., $1 + 2/e \exp[E^e - 2E^C/(k_B T)w]$, can be approximated as 1. Therefore, when only one disconnection mode is activated, Eq. (6) can be simplified as

$$M = \frac{2\omega\delta w h^2}{k_B T} \exp\left(-\frac{E^* + E^C}{k_B T/w}\right). \quad (7)$$

Indeed, both Eqs. (7) and (5) share a similar form, with the activation energy Q in Eq. (5) corresponding to the combined energy barrier for disconnection nucleation E^C and migration E^* in Eq. (7).

Both theories indicate that the antithermal behavior of GB mobility is a result of the first term $1/k_B T$, which arises from the inequality of the activation energy for GB to move forth (Q) and back $(Q + \Psi)$ as illustrated in Fig. 7(a). This inequality of the activation energy is inherent to GB migration and contributes to the antithermal behavior observed. This aligns with our observation that the transition in thermal behavior of GB mobility is not solely attributed to changes in the migration mode, as supported by the analysis of the shear coupling factor (Figs. 3 and 5).

B. Activation energy for GB migration

In Eq. (5), the activation energy Q for GB migration plays a crucial role in deciding the thermal behavior of the GB migration. By setting the derivative of Eq. (5) with respect to T equal to zero, i.e., $M' = 0$, we can get

$$Q = k_B T_{\text{trans}}. \quad (8)$$

Equation (8) suggests a linear relationship between Q and T_{trans} by theory, which means that if we know the activation energy Q, the thermal behavior of the GB is predictable. But the question falls on how to determine the activation energy of the GB?

According to Chen *et al.* [7], the activation energy Q in Eq. (5) is linked to the energy required for disconnection nucleation and migration [as shown in Eq. (7)]; the latter can be determined by performing NEB analysis [7,43,44]. Therefore, the energy barriers of nine GBs listed in Table I are calculated through NEB method, and the maximum height of the energy barrier E was extracted, as shown in Fig. 8(a). It is important to note that the E is reported as normalized values by dividing each energy barrier by the respective GB area to eliminate the possible size effect of NEB simulation.

Alternatively, by examining Eq. (5), one can deduce that

$$\ln M = -\frac{Q}{k_B T}\left(1 + \frac{k_B T \ln T}{Q}\right) + A \quad (9)$$

where A is a constant. When $k_B T \ln T \ll Q$, i.e., $T \ll T_{\text{trans}}$, the terms in the bracket becomes 1, and the GB mobility M exhibits Arrhenius behavior, as shown in Fig. 3(d), and therefore, in this temperature range the apparent activation energy Q can be calculated by fitting the slope of the $\ln M - 1/k_B T$ line. The calculated E and Q are listed in Table I. Figure 8(b) shows that, even though with different values, E and Q exhibit a linear relationship. Besides, both E and Q exhibit a linear relationship with T_{trans} as predicted by Eq. (8), as shown in Figs. 8(c) and 8(d). It is worth noting that the slope of fitted Q-T line is 7.4687×10^{-5} eV/K which is very close to the $k_B = 8.6173 \times 10^{-5}$ eV/K, further validating the classical thermal-activation model [24].

Indeed, there are limitations to both methods when calculating the activation energy for GB migration. In the classical thermal-activation model, the fitted apparent activation energy Q assumes that the temperature T is much smaller than T_{trans}. However, in cases where the GB exhibits antithermal behavior, the value of T_{trans} is typically small, making it difficult to satisfy the condition $T \ll T_{\text{trans}}$. Additionally, obtaining accurate M-T curves at extremely low temperatures can be challenging. Therefore, using the Arrhenius approximation in such cases may introduce potential errors. On the other hand, the energy barrier E calculated using the NEB method has its own limitations. The NEB calculation result strongly depends on the size of the model used, whereas the activation energy for GB migration should be independent of the model size. Moreover, some GBs exhibit a two-step migration process with two energy barriers [Fig. 8(a)], and apparently one of them is more closely related to the activation energy [Figs. 8(b) and 8(c)]. This two-step process has been observed before in the literature [51], but the physical mechanisms behind it are still unclear. Nevertheless, there are advantages to using E. First, it can be accurately calculated, providing a reliable estimate of the energy barrier. Second, it does not require fitting data across a wide range of temperatures, which can be challenging to obtain. Therefore, E can serve as a useful indicator for predicting the activation energy and thermal behavior of GB migration.

C. Effect of the driving force on the thermal behavior of GB migration

To investigate the impact of driving force on GB migration, we modified the synthetic driving force code [6] in LAMMPS to be invoked during the energy minimization process. This
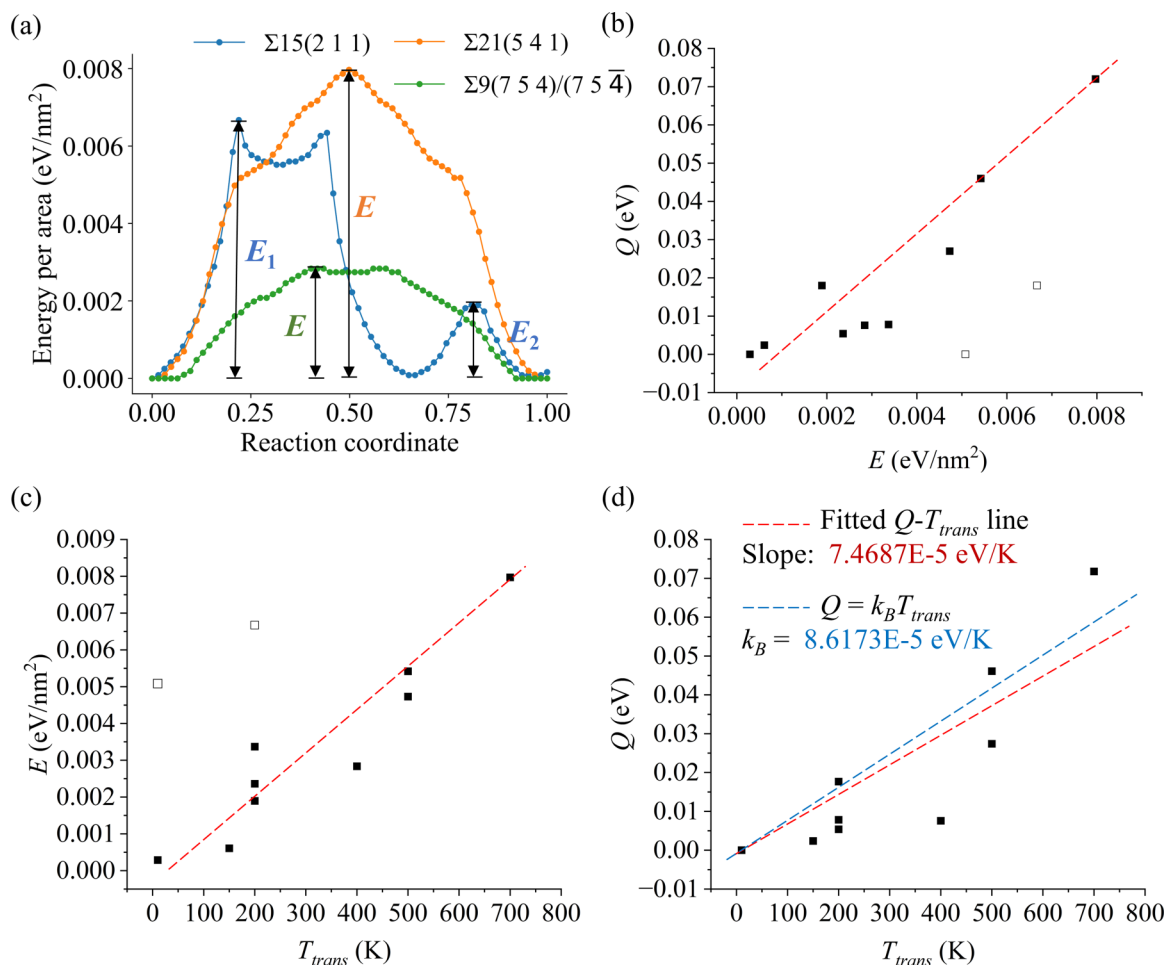
FIG. 8. (a) the energy barrier E measured from NEB simulations, and (b) the comparison between E and the apparent activation energy Q. (c), (d) Plot of (c) E and (d) Q vs. GB thermal behavior transition temperature T_{trans} ($\square$ indicates the second energy barrier E for GBs with two distinct energy barriers).

enabled us to calculate the energy barrier E for GB migration under the influence of synthetic driving forces φ. As a comparison, we also examined the effect of shear stress τ on E, and an analysis based on the recently proposed concept of GB mobility tensor [14,52,53] (see the Supplemental Material [39] for details) revealed that, for causing GB migration at the same mode and at the same velocity, the φ and τ should satisfy the relation $\tau = \varphi/\beta$. Figure 9(a) demonstrates that both the φ and τ can reduce the E, and their effects are equivalent. Therefore, for simplicity, our subsequent analysis primarily focused on the φ.

In Fig. 9(b), it is observed that as the driving force increases, the E exhibits a monotonic decrease. This observation is consistent with the decreasing trend of the apparent activation energy Q as the driving force increases, as shown in Fig. 9(c). Moreover, the driving force at which the E reaches zero in Fig. 9(b) coincides with T_{trans} reaching 0 K in Fig. 4, as predicted by Eq. (8). This finding explains the shift of the T_{trans} towards lower temperatures with the increase of the driving force.

The mechanisms discussed above, along with the observations presented in Fig. 5, provide an explanation for the different thermal behaviors exhibited by GBs under varying

driving force conditions. When the driving force is low, T_{trans} exhibits a linear relationship with the migration activation energy Q. The driving force influences T_{trans} by modifying Q, thereby altering the thermal behavior of GB migration. Additionally, a large driving force can activate more migration modes at a lower temperature, which can also change the thermal behavior of GB migration, such as transitioning from antithermal to thermally activated behavior [Fig. 4(a)].

Another notable observation is that in Fig. 9(b), most of the energy barriers reach zero before the applied synthetic driving force reaches 44.1 MPa. While this value is close to the maximum driving force typically used in experimental situations, it is still relatively small in MD simulations to observe obvious GB migration within a nanosecond time scale. It is worth considering that GBs exhibiting antithermal behavior often have small energy barriers for migration, as confirmed by Homer *et al.* [24]. Therefore, the driving forces used in previous studies [10,11,24] on GB thermal behavior, such as 73.5 MPa and above, may be too large and could have already caused significant changes in the GB migration mechanisms. Furthermore, since the same driving force has different effects on the migration energy barrier in different GBs [Fig. 9(b)], future studies should consider additional factors. Ideally, the
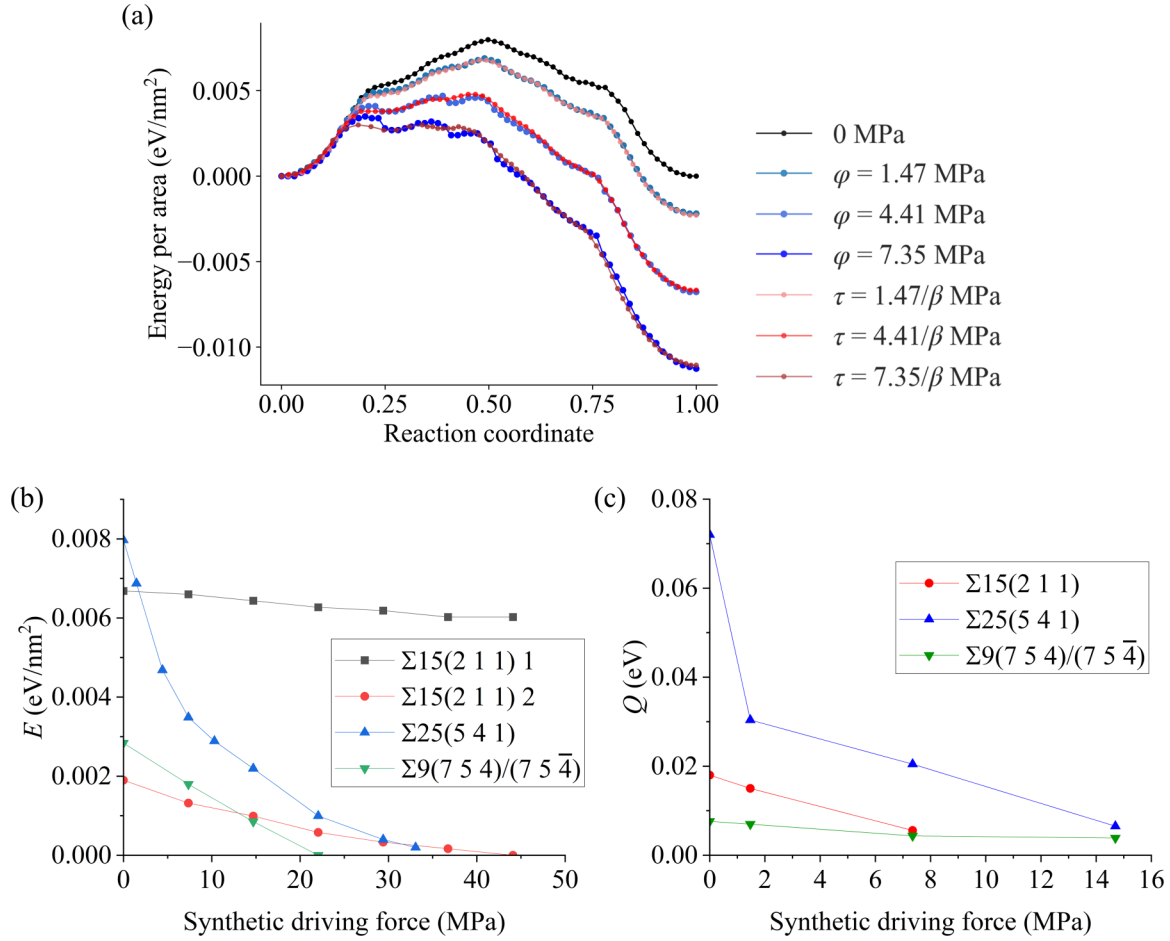
FIG. 9. (a) The effect of synthetic driving force φ and shear stress τ on the energy barrier of migration E for the $\Sigma21(5\ 4\ 1)$ GB. (b) Variation of E with synthetic driving force for $\Sigma15\ (2\ 1\ 1)$, $\Sigma9\ (7\ 5\ 4)/(7\ 5\ \overline{4})$, and $\Sigma21(5\ 4\ 1)$ GBs. (c) Apparent activation energy Q as a function of synthetic driving force for the respective GBs. (Note that the tracking of Q in (c) is limited to a maximum external driving force of 14.7 MPa due to the difficulty in performing Arrhenius fitting at extremely low temperatures.)

driving force should not exceed the critical value at which the first energy barrier is eliminated if one wishes to explore the GB behavior under typical experimental conditions.

When the driving force reaches extremely high magnitudes, the energy term Ψ introduced by the driving force in Eq. (4) becomes significant and cannot be ignored. By directly referring to Eq. (4), the GB mobility can be expressed as follows:

$$M = \frac{v}{p} = Nbv\exp\left(\frac{-Q}{k_BT}\right)\left[1 - \exp\left(\frac{-\Psi}{k_BT}\right)\right]\Big/P. \quad (10)$$

By fitting the data of $\Sigma21(5\ 4\ 1)$ GB in Fig. 9(b), it was found that M decreases exponentially with the driving force P, as shown in the inset of Fig. 10. Assuming that the activation energy for GB migration follows the same functional dependence on P as E does, and considering that Ψ is proportional to P, all energy terms in Eq. (10) can be expressed in terms of P:

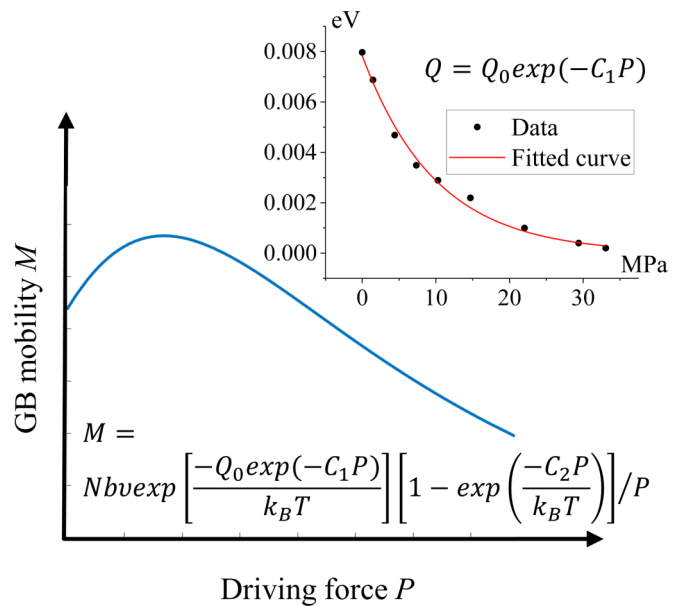$$Q = Q_0\exp(-C_1P), \quad (11)$$

$$\Psi = C_2P. \quad (12)$$

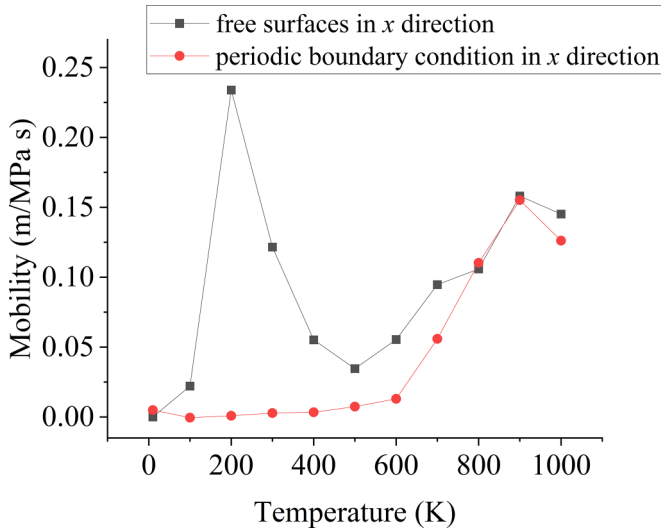FIG. 10. Plot of GB mobility M vs. driving force P based on Eq. (10).

FIG. 11. Comparison of the mobility vs. temperature curves for $\Sigma 15(2\ 1\ 1)$ GB under different boundary conditions.

Here, Q_0 is the initial activation energy when the driving force is 0; C_1 and C_2 are fitted constants. By incorporating these equations into Eq. (10), we can observe from Fig. 10 that the GB mobility M initially increases with P, reaching a peak and then decreasing as P further increases. This behavior aligns with the antidriving force phenomenon observed at low temperatures in Fig. 6. At high temperatures, where $k_B T$ is much larger than both Q and Ψ, M becomes a constant and independent of P, which is consistent with the findings in Fig. 6. These observations indicate that both the driving force and temperature have a similar effect on GB mobility, and this effect can be described and unified using Eq. (10).

Although the analysis presented so far is based on the synthetic driving force, the comparable effects observed for synthetic driving force and shear stress [Fig. 9(a)] suggest that these findings should also apply to shear stress conditions.

D. Limitations of the current model

Our study is conducted on an ideal bicrystal system with open ends, which provides a controlled environment to examine the influence of temperature and driving force on GB migration. However, in actual polycrystalline materials, the presence of neighboring grains introduces additional constraints that can impact GB migration behavior. To investigate this, we altered the boundary condition in the x direction from free surface to periodic and conducted random walk simulations. The results presented in Fig. 11 reveal that changing the boundary condition in the x direction from free surface to periodic has a significant effect on GB mobility. Below 600 K, the GB migration is completely restricted, indicating that the presence of neighboring grains imposes constraints that hinder the GB migration. However, as the temperature increases to 800 K, the GB mobilities under both boundary conditions become equal again. This observation aligns with the findings reported by Schratt and Mohles [48]. The concept of reconciling grain growth, as investigated by Thomas *et al.* [54], provides an explanation for this phenomenon. At low temperatures, when only one disconnection mode with strong

shear coupling dominates GB migration, the constraints imposed by neighboring grains inhibit the GB migration process. However, at higher temperatures, where multiple migration modes are activated, the constraints can be alleviated by alternatively activating modes with opposite shear coupling signs.

Indeed, the results presented in Fig. 11 do not contradict the conclusions drawn from the bicrystal model with shrink-wrapped boundary conditions. The constraints imposed by surrounding grains can be considered as an opposite driving force that restricts GB migration by increasing the activation energy required for GB migration, leading to a significant increase in the T_{trans}. Besides, it should be noted that in realistic situations, grains are often much larger than the model used in our study. Consequently, the presence of large grains adjacent to the GB can store a significant amount of elastic energy, mitigating the constraints imposed by neighboring grains. Additionally, real grains possess various mechanisms to alleviate these constraints, including GB rotation [55–57] and the migration of triple junctions [58,59]. Therefore, despite the simplifications inherent in the bicrystal system, studying it remains informative and provides valuable reference for understanding GB behavior in real-world cases.

Another limitation of the classical thermal-activation model is its assumption that only one migration mode dominates GB migration. However, in polycrystalline materials, the phenomenon of reconciling GB migration necessitates the consideration of multiple migration modes [54]. Disconnection theory [30] proposes that multiple modes can be simultaneously activated at different locations along the GB in the form of disconnections, which are line defects combining step height and dislocation characteristics. This assumption has been supported by experimental observations [60]. Chen *et al.* [7] hypothesize that the GB mobility is the sum of the mobilities of each mode, expressed as

$$M = \sum_m M_m. \tag{13}$$

Here, M_m represents the mobility equation [Eq. (5)] for the mth migration mode. However, accurately measuring the constant terms and activation energies in Eq. (5) for all the modes remains a challenge.

V. CONCLUSION

By conducting systematic atomistic simulations of GB migration using both dynamic and static approaches, we have derived several key conclusions:

The antithermal behavior of GB mobility is an intrinsic nature of GBs, and the transition temperature (T_{trans}) in thermal behavior, at which the mobility of GB is at its maximum, exhibits a linear relationship with the activation energy for GB migration. This finding provides support for both Homer's classical thermal-activation model [24,25] [Eq. (5)] and Chen *et al.*'s disconnection-based theory [7] [Eq. (7)].

The synthetic driving force can reduce the activation energy required for GB migration, leading to a shift in the transition temperature (T_{trans}) to lower values. Moreover, a higher driving force can activate more migration modes at lower temperatures, thereby influencing the thermal behavior of the GB. We suggest an optimal range of driving forces that

should be considered in future atomistic simulations investigating the GB thermal behavior under typical experimental conditions.

Through our quantitative analysis of the effects of the synthetic driving force and shear stress on the energy barrier for GB migration, we have observed that these two driving forces are equivalent in their ability to lower the energy barrier. This means that the conclusions drawn from studying the synthetic driving force can also be applied to the case of shear stress.

We have refined the thermal-activation model by incorporating the influence of the driving force on the activation energy. This modified model accurately captures the observed antidriving force trend in GB mobility resulting from changes in the driving force.

These findings contribute to our understanding of GB migration and provide insights into the interplay between temperature, driving force, and GB mobility, which is essential for GB engineering and modern industry.

[1] M. Upmanyu, D. J. Srolovitz, L. S. Shvindlerman, and G. Gottstein, Misorientation dependence of intrinsic grain boundary mobility: Simulation and experiment, Acta Mater. **47**, 3901 (1999).

[2] A. D. Rollett, G. Gottstein, L. S. Shvindlerman, and D. A. Molodov, Grain boundary mobility–A brief review, Int. J. Mater. Res. **95**, 226 (2004).

[3] T. O. E. Skinner, D. G. A. L. Aarts, and R. P. A. Dullens, Grain-Boundary Fluctuations in Two-Dimensional Colloidal Crystals, Phys. Rev. Lett. **105**, 168301 (2010).

[4] P. R. Cantwell, E. A. Holm, M. P. Harmer, and M. J. Hoffmann, Anti-thermal behavior of materials, Scr. Mater. **103**, 1 (2015).

[5] D. L. Olmsted, E. A. Holm, and S. M. Foiles, Survey of computed grain boundary properties in face-centered cubic metals—II: Grain boundary mobility, Acta Mater. **57**, 3704 (2009).

[6] K. G. Janssens, D. Olmsted, E. A. Holm, S. M. Foiles, S. J. Plimpton, and P. M. Derlet, Computing the mobility of grain boundaries, Nat. Mater. **5**, 124 (2006).

[7] K. Chen, J. Han, and D. J. Srolovitz, On the temperature dependence of grain boundary mobility, Acta Mater. **194**, 412 (2020).

[8] E. R. Homer, E. A. Holm, S. M. Foiles, and D. L. Olmsted, Trends in grain boundary mobility: Survey of motion mechanisms, JOM **66**, 114 (2014).

[9] Z. T. Trautt, M. Upmanyu, and A. Karma, Interface mobility from interface random walk, Science **314**, 632 (2006).

[10] J. L. Priedeman, D. L. Olmsted, and E. R. Homer, The role of crystallography and the mechanisms associated with migration of incoherent twin grain boundaries, Acta Mater. **131**, 553 (2017).

[11] J. L. Bair and E. R. Homer, Antithermal mobility in Σ7 and Σ9 grain boundaries caused by stick-slip stagnation of ordered atomic motions about coincidence site lattice atoms, Acta Mater. **162**, 10 (2019).

[12] J. Humberson and E. A. Holm, Anti-thermal mobility in the Σ3 [111]60°{11 8 5} grain boundary in nickel: Mechanism and computational considerations, Scr. Mater. **130**, 1 (2017).

[13] A. Karma, Z. T. Trautt, and Y. Mishin, Relationship between Equilibrium Fluctuations and Shear-Coupled Motion of Grain Boundaries, Phys. Rev. Lett. **109**, 095501 (2012).

[14] K. Chen, J. Han, X. Pan, and D. J. Srolovitz, The Grain Boundary Mobility Tensor, Proc. Natl. Acad. Sci. USA **117**, 4533 (2020).

[15] J. Han, V. Vitek, and D. J. Srolovitz, The grain-boundary structural unit model redux, Acta Mater. **133**, 186 (2017).

[16] A. D. Banadaki and S. Patala, A three-dimensional polyhedral unit model for grain boundary structure in Fcc metals, Npj Comput. Mater. **3**, 13 (2017).

[17] M. Wagih, P. M. Larsen, and C. A. Schuh, Learning grain boundary segregation energy spectra in polycrystals, Nat. Commun. **11**, 6376 (2020).

[18] X. Song and C. Deng, Atomic energy in grain boundaries studied by machine learning, Phys. Rev. Mater. **6**, 043601 (2022).

[19] Z. Jin, X. Li, and K. Lu, Formation of Stable Schwarz Crystals in Polycrystalline Copper at the Grain Size Limit, Phys. Rev. Lett. **127**, 136101 (2021).

[20] J. E. Burke and D. Turnbull, Recrystallization and grain growth, Prog. Met. Phys. **3**, 220 (1952).

[21] K. Zhang, J. R. Weertman, and J. A. Eastman, Rapid stress-driven grain coarsening in nanocrystalline Cu at ambient and cryogenic temperatures, Appl. Phys. Lett. **87**, 061921 (2005).

[22] X. Shi and J. Luo, Decreasing the Grain Boundary Diffusivity in Binary Alloys with Increasing Temperature, Phys. Rev. Lett. **105**, 236102 (2010).

[23] W. Rheinheimer and M. J. Hoffmann, Non-arrhenius behavior of grain growth in strontium titanate: New evidence for a structural transition of grain boundaries, Scr. Mater. **101**, 68 (2015).

[24] E. R. Homer, O. K. Johnson, D. Britton, J. E. Patterson, E. T. Sevy, and G. B. Thompson, A classical equation that accounts for observations of non-arrhenius and cryogenic grain boundary migration, Npj Comput. Mater. **8**, 157 (2022).

[25] G. Gottstein and L. S. Shvindlerman, *Grain Boundary Migration in Metals: Thermodynamics, Kinetics, Applications* (CRC, Boca Raton, 2009).

[26] T. Frolov, D. L. Olmsted, M. Asta, and Y. Mishin, Structural phase transformations in metallic grain boundaries, Nat. Commun. **4**, 1899 (2013).

[27] T. Meiners, T. Frolov, R. E. Rudd, G. Dehm, and C. H. Liebscher, Observations of grain-boundary phase transformations in an elemental metal, Nature (London) **579**, 375 (2020).

[28] D. L. Olmsted, S. M. Foiles, and E. A. Holm, Grain boundary interface roughening transition and its effect on grain boundary mobility for non-faceting boundaries, Scr. Mater. **57**, 1161 (2007).

[29] K. Chen, D. J. Srolovitz, and J. Han, Grain-boundary topological phase transitions, Proc. Natl. Acad. Sci. USA **117**, 33077 (2020).

[30] J. Han, S. L. Thomas, and D. J. Srolovitz, Grain-boundary kinetics: A unified approach, Prog. Mater. Sci. **98**, 386 (2018).

[31] D. L. Olmsted, S. M. Foiles, and E. A. Holm, Survey of computed grain boundary properties in face-centered cubic metals: I. grain boundary energy, Acta Mater. **57**, 3694 (2009).

[32] C. Deng and C. A. Schuh, Diffusive-to-ballistic transition in grain boundary motion studied by atomistic simulations, Phys. Rev. B **84**, 214102 (2011).

[33] C. Deng and C. A. Schuh, Atomistic Simulation of Slow Grain Boundary Motion, Phys. Rev. Lett. **106**, 045503 (2011).

[34] M. I. Mendelev, C. Deng, C. A. Schuh, and D. J. Srolovitz, Comparison of molecular dynamics simulation methods for the study of grain boundary migration, Model. Simul. Mater. Sci. Eng. **21**, 045017 (2013).

[35] T. Yu, I. Chesser, S. Ratanaphan, E. Holm, S. Yang, and C. Deng, Survey of shear coupling behavior in Fcc Ni and Bcc Fe grain boundaries, Materialia **15**, 100945 (2021).

[36] G. Henkelman, B. P. Uberuaga, and H. Jónsson, A climbing image nudged elastic band method for finding saddle points and minimum energy paths, J. Chem. Phys. **113**, 9901 (2000).

[37] G. Henkelman and H. Jónsson, Improved tangent estimate in the nudged elastic band method for finding minimum energy paths and saddle points, J. Chem. Phys. **113**, 9978 (2000).

[38] E. Maras, O. Trushin, A. Stukowski, T. Ala-Nissila, and H. Jonsson, Global transition path search for dislocation formation in Ge on Si (001), Comput. Phys. Commun. **205**, 13 (2016).

[39] See Supplemental Material at http://link.aps.org/supplemental/10.1103/PhysRevMaterials.7.093401 for the method to calculate the energy barrier for GB migration; dichromatic pattern analysis for $\Sigma15$ (2 1 1), $\Sigma21$ (5 4 1), and $\Sigma9$ (7 5 4)/(7 5 4) GBs; plots of GB mobility vs temperature curves of GBs in Table I determined by random walk method; GB mobility of $\Sigma15$ (2 1 1), $\Sigma21$ (5 4 1), and $\Sigma9$ (7 5 4)/(7 5 4) GBs under varying synthetic driving forces (58.8–440.97 MPa) and temperatures; and derivation of equivalent shear stress and synthetic driving force from the GB mobility tensor.

[40] A. Kushima, X. Lin, J. Li, J. Eapen, J. C. Mauro, X. Qian, P. Diep, and S. Yip, Computing the viscosity of supercooled liquids, J. Chem. Phys. **130**, 224504 (2009).

[41] P. Cao, M. Li, R. J. Heugle, H. S. Park, and X. Lin, Self-learning metabasin escape algorithm for supercooled liquids, Phys. Rev. E **86**, 016710 (2012).

[42] P. Cao, X. Lin, and H. S. Park, Strain-rate and temperature dependence of yield stress of amorphous solids via a self-learning metabasin escape algorithm, J. Mech. Phys. Solids **68**, 239 (2014).

[43] A. Rajabzadeh, F. Mompiou, M. Legros, and N. Combe, Elementary Mechanisms of Shear-Coupled Grain Boundary Migration, Phys. Rev. Lett. **110**, 265507 (2013).

[44] N. Combe, F. Mompiou, and M. Legros, Disconnections kinks and competing modes in shear-coupled grain boundary migration, Phys. Rev. B **93**, 024109 (2016).

[45] S. Plimpton, Fast parallel algorithms for short-range molecular dynamics, J. Comput. Phys. **117**, 1 (1995).

[46] S. M. Foiles and J. J. Hoyt, Computation of grain boundary stiffness and mobility from boundary fluctuations, Acta Mater. **54**, 3351 (2006).

[47] F. Ulomek, C. J. O'Brien, S. M. Foiles, and V. Mohles, Energy conserving orientational force for determining grain boundary mobility, Model. Simul. Mater. Sci. Eng. **23**, 025007 (2015).

[48] A. A. Schratt and V. Mohles, Efficient calculation of the ECO driving force for atomistic simulations of grain boundary motion, Comput. Mater. Sci. **182**, 109774 (2020).

[49] F. M. Dekking, C. Kraaikamp, H. P. Lopuhaä, and L. E. Meester, *A Modern Introduction to Probability and Statistics: Understanding Why and How* (Springer, New York, 2005), Vol. 488.

[50] C. P. Race, J. von Pezold, and J. Neugebauer, Role of the mesoscale in migration kinetics of flat grain boundaries, Phys. Rev. B **89**, 214110 (2014).

[51] F. Ulomek and V. Mohles, Separating grain boundary migration mechanisms in molecular dynamics simulations, Acta Mater. **103**, 424 (2016).

[52] L. Onsager, Reciprocal relations in irreversible processes, Phys. Rev. **37**, 405 (1931).

[53] D. G. Miller, Thermodynamics of irreversible processes. The experimental verification of the onsager reciprocal relations, Chem. Rev. **60**, 15 (1960).

[54] S. L. Thomas, K. Chen, J. Han, P. K. Purohit, and D. J. Srolovitz, Reconciling grain growth and shear-coupled grain boundary migration, Nat. Commun. **8**, 1764 (2017).

[55] L. Wang, J. Teng, P. Liu, A. Hirata, E. Ma, Z. Zhang, M. Chen, and X. Han, Grain rotation mediated by grain boundary dislocations in nanocrystalline platinum, Nat. Commun. **5**, 4402 (2014).

[56] Y. B. Wang, B. Q. Li, M. L. Sui, and S. X. Mao, Deformation-induced grain rotation and growth in nanocrystalline Ni, Appl. Phys. Lett. **92**, 011903 (2008).

[57] Z. Kou, Y. Yang, L. Yang, X. Luo, and B. Huang, Observing the dynamic rotation and annihilation process of an isolated nanograin at the atomic scale in Al, Mater. Charact. **147**, 311 (2019).

[58] S. L. Thomas, C. Wei, J. Han, Y. Xiang, and D. J. Srolovitz, Disconnection description of triple-junction motion, Proc. Natl. Acad. Sci. USA **116**, 8756 (2019).

[59] M. Aramfard and C. Deng, Influences of triple junctions on stress-assisted grain boundary motion in nanocrystalline materials, Model. Simul. Mater. Sci. Eng. **22**, 055012 (2014).

[60] Q. Zhu, G. Cao, J. Wang, C. Deng, J. Li, Z. Zhang, and S. X. Mao, *In situ* atomistic observation of disconnection-mediated grain boundary migration, Nat. Commun. **10**, 156 (2019).